J|A|C|S
ARTICLES
Published on Web 03/23/2002

Oxygen-Transfer Reactions between 3d Transition Metals and N_2O and NO_2

András Stirling*,†

Contribution from the Institute of Isotope and Surface Chemistry, Chemical Research Center, Hungarian Academy of Sciences, P.O. Box 77, Budapest H-1525, Hungary

Received August 6, 2001. Revised Manuscript Received November 19, 2001

Abstract: Density functional calculations have been performed to describe reactions of ground-state 3d transition metal atoms (Sc−Ni) with N_2O and NO_2 molecules. From the analysis of the calculated reaction surfaces, a general reaction mechanism evolved. The reactions are initiated by electron transfer from metal to the oxidant molecule, which weakens the N−O bond and facilitates an $O^-(^2P)$ abstraction. 4s−3d hybridization taking place in the metal electronic structure plays an essential role in the net $4s^\beta$ electron transfer from the metal atom to the nitrogen−oxide molecule. These key steps contribute to connect the reactant and product channels on a single potential energy surface. The calculations revealed that reaction with NO_2 yields stable oxo−nitrosyl insertion products, and their equilibrium structural properties can be understood by inspecting the $4\pi^*$ metal−oxide orbital occupancies. Correlation is obtained between the metal 3d ionization energies and the reaction rates as well as activation energies. This correlation provides additional support for the reaction mechanism called *electron-transfer-assisted oxygen abstraction*. This novel mechanism exhibits the basic features of the simple *electron transfer* and *direct abstraction* kinetic models and sheds new light on the so-called *resonance interaction* model as well.

I. Introduction

Reactions of transition metal (TM) atoms with small nitrogen−oxide molecules are of great experimental and theoretical significance.[1−36] The underlying reaction mechanism plays roles in several fields of chemistry, such as the catalytic decomposition of the NO_x molecules, the chemistry of the atmosphere, and the oxidation of the transition metals. It has been found experimentally that the transition metal atoms cleave the N−O bond of both N_2O and NO_2 and form the corresponding metal−oxide molecule according to the following reaction equations:

$$M + N_2O \rightarrow MO + N_2 \quad (1)$$

$$M + NO_2 \rightarrow MO + NO \quad (2)$$

Two main types of experiment have been carried out to investigate these reactions: beam−gas and beam−beam arrangements, and low-pressure gas reactor experiments with chemiluminescence or laser-induced fluorescence detection techniques. Reaction 1 has been measured for all 3d TMs,[5−10,12,13,16−18,21,24,28,29,32,33] whereas reaction 2 has been studied in detail only for Sc,[3,4] Ti,[2,12] V,[1] and Fe.[29] It has been found that these reactions show interestingly varied behavior. In particular, for NO_2 the bimolecular oxygen abstraction reactions were measured to be fast even with ground-state atoms. Moreover, the reactions were found to be temperature independent under 1000 K, which implies no activation energy. For N_2O it has been revealed that the reactions are also bimolecular

* To whom correspondence should be addressed. E-mail: stirling@cscs.ch.

† Present address: CSCS-Swiss Center for Scientific Computing, Via Cautouale, Manno 6928 Switzerland.

(1) Jones, R. W.; Gole, J. L. *J. Chem. Phys.* **1976**, *65*, 3800.
(2) Dubois, L. H.; Gole, J. L. *J. Chem. Phys.* **1977**, *66*, 779.
(3) Gole, J. L.; Preuss, D. R. *J. Chem. Phys.* **1977**, *66*, 3000.
(4) Gole, J. L.; Pace, S. A. *J. Chem. Phys.* **1980**, *73*, 836.
(5) Ritter, D.; Weisshaar, J. C. *J. Phys. Chem.* **1989**, *93*, 1576.
(6) Ritter, D.; Weisshaar, J. C. *J. Phys. Chem.* **1990**, *94*, 4907.
(7) Levy, M. R. *J. Phys. Chem.* **1989**, *93*, 5195.
(8) Mitchell, S. A.; Hackett, P. A. *J. Chem. Phys.* **1990**, *93*, 7813.
(9) Mitchell, S. A.; Hackett, P. A. *J. Chem. Phys.* **1990**, *93*, 7822.
(10) Mark Parnis, J.; Mitchell, S. A.; Hackett, P. A. *J. Phys. Chem.* **1990**, *94*, 8152.
(11) McClean, R. E.; Pasternack, L. *J. Phys. Chem.* **1992**, *96*, 9828.
(12) Campbell, M. L.; McClean, R. E. *J. Phys. Chem.* **1993**, *97*, 7942.
(13) Clemmer, D. E.; Honma, K.; Koyano, I. *J. Phys. Chem.* **1993**, *97*, 11480.
(14) Campbell, M. L.; McClean, R. E. *J. Chem. Soc., Faraday Trans.* **1995**, *91*, 3787.
(15) Campbell, M. L. *J. Chem. Soc., Faraday Trans.* **1996**, *92*, 4377.
(16) Campbell, M. L. *J. Chem. Phys.* **1996**, *104*, 7515.
(17) Campbell, M. L.; Metzger, J. R. *Chem. Phys. Lett.* **1996**, *253*, 158.
(18) Plane, J. M. C.; Rollason, R. J. *J. Chem. Soc., Faraday Trans.* **1996**, *92*, 4371.
(19) McClean, R. E.; Campbell, M. L.; Goodwin, R. H. *J. Phys. Chem.* **1996**, *100*, 7502.
(20) Campbell, M. L. *J. Phys. Chem.* **1996**, *100*, 19430.
(21) Campbell, M. L.; Hooper, K. L.; Kölsch, E. J. *Chem. Phys. Lett.* **1997**, *274*, 7.
(22) Campbell, M. L.; Hooper, K. L. *J. Chem. Soc., Faraday Trans.* **1997**, *93*, 2139.
(23) McClean, R. E.; Campbell, M. L.; Kölsch, E. J. *J. Phys. Chem. A* **1997**, *101*, 3348.
(24) Matsui, R.; Senba, K.; Honma, K. *J. Phys. Chem. A* **1997**, *101*, 179.
(25) Campbell, M. L. *J. Chem. Soc., Faraday Trans.* **1998**, *94*, 353.
(26) Campbell, M. L. *J. Chem. Soc., Faraday Trans.* **1998**, *94*, 1687.
(27) Campbell, M. L. *Chem. Phys. Lett.* **1998**, *294*, 339.
(28) Honma, K. *J. Phys. Chem. A* **1999**, *103*, 1809.
(29) Plane, J. M. C.; Rollason, R. J. *Phys. Chem. Chem. Phys.* **1999**, *1*, 1843.
(30) Campbell, M. L. *J. Chem. Phys.* **1999**, *111*, 562.
(31) Vinckier, C.; Helaers, J.; Christiaens, P.; Remeysen, J. *J. Phys. Chem. A* **1999**, *103*, 11321.
(32) Vetter, R.; Naulin, C.; Costes, M. *Phys. Chem. Chem. Phys.* **2000**, *2*, 643.
(33) Campbell, M. L.; Kölsch, E. J.; Hooper, K. L. *J. Phys. Chem. A* **2000**, *104*, 11147.
(34) Futerko, P. M.; Fontijn, A. *J. Chem. Phys.* **1991**, *95*, 8065.
(35) Futerko, P. M.; Fontijn, A. *J. Chem. Phys.* **1992**, *97*, 3861.
(36) Futerko, P. M.; Fontijn, A. *J. Chem. Phys.* **1993**, *98*, 7004.

10.1021/ja0118946 CCC: $22.00

Table 1. Experimental Electronic Configurations of the 3d Transition Metal Atoms in Atomic and Oxide Form As Compiled from Refs 54 and 71 (Electron Terms and Multiplicities Are in Parentheses)

	isolated atom			metal–oxide ground state				
				atomic asymptotes				
				neutral		ionic		oxide
metal	ground state	first excited state	ionic ground state	metal	oxygen	metal	oxygen	multiplicity
Sc	s^2d^1 (^{2}D)	s^1d^2 (^{4}F)	s^1d^1 (^{3}D)	s^1d^2 ($M = 4$)	(^{3}P)	s^1d^1 ($M = 3$)	(^{2}P)	($M = 2$)
Ti	s^2d^2 (^{3}F)	s^1d^3 (^{5}F)	s^1d^2 (^{4}F)	s^1d^3 ($M = 5$)	(^{3}P)	s^1d^2 ($M = 4$)	(^{2}P)	($M = 3$)
V	s^2d^3 (^{4}F)	s^1d^4 (^{6}D)	d^4 (^{5}D)	s^1d^4 ($M = 6$)	(^{3}P)	s^1d^3 ($M = 5$)	(^{2}P)	($M = 4$)
Cr	s^1d^5 (^{7}S)	s^2d^4 (^{5}D)	d^5 (^{6}S)	s^1d^5 ($M = 7$)	(^{3}P)	s^1d^4 ($M = 6$)	(^{2}P)	($M = 5$)
Mn	s^2d^5 (^{6}S)	s^1d^6 (^{6}D)	s^1d^5 (^{7}S)	s^1d^6 ($M = 6$)	(^{1}D)	s^1d^5 ($M = 7$)	(^{2}P)	($M = 6$)
Fe	s^2d^6 (^{5}D)	s^1d^7 (^{5}F)	s^1d^6 (^{6}D)	s^1d^7 ($M = 5$)	(^{1}D)	s^1d^6 ($M = 6$)	(^{2}P)	($M = 5$)
Co	s^2d^7 (^{4}F)	s^1d^8 (^{4}F)	d^8 (^{3}F)	s^2d^7 ($M = 4$)	(^{1}D)	s^2d^6 ($M = 5$)	(^{2}P)	($M = 4$)
Ni	s^2d^8 (^{3}D)[a]	s^1d^9 (^{3}F)	d^9 (^{2}D)	s^2d^8 ($M = 3$)	(^{1}D)	s^2d^7 ($M = 4$)	(^{2}P)	($M = 3$)

[a] If averaging over the spin−orbit components, the Ni ground state becomes s^1d^9.

processes with large reaction enthalpies. Despite the large reaction heat, these reactions are inefficient and usually slow, as opposed to, e.g., reactions with NO_2 or SO_2. Temperature-dependent measurements revealed activation energies within the 2−10 kcal/mol domain which are significant compared to the RT value at room temperature (0.6 kcal/mol). Excited-state metal atoms were found to react easily.

Three reaction mechanisms have been proposed to explain these observations. In the electron-transfer (ET) mechanism,[5,6,37] the key step is an electron transfer from the metal atom to the N_2O molecule following the harpoon mechanism.[37] The electron transfer takes place at a certain distance when the energy of the Coulomb interaction between the M^+ and N_2O^- ions can cover the energy difference between the metal ionization and the N_2O electronaffinity potentials (see Figure 1a). The crossing point (R) and the cross section ($R^2\pi$) can be estimated by using the formula

$$R = e^2/[4\pi\epsilon_0(\mathrm{IE} - \mathrm{EA})] \qquad (3)$$

where e is the electron charge, $4\pi\epsilon_0$ is the permittivity, IE is the ionization energy, and EA is the electron affinity. The mechanism is in accordance with the higher reactivity of the excited metal atoms because the ionization is easier for these states, which increases the cross section of the reaction. The direct abstraction (DA) mechanism (also called the surface crossing model)[5,6] assumes that a neutral oxygen atom is abstracted from the N_2O. Since the ground state of the 3d TM atoms (from Sc to Ni) is usually $4s^23d^n$ (except Cr), while in the corresponding oxide the state of the metal atom correlates asymptotically with the $4s^13d^{n+1}$ configuration (except Co and Ni), this mechanism assumes that the reaction path goes over a barrier when the $4s^23d^n$ and the $4s^13d^{n+1}$ surfaces cross (see Figure 1b; for the atomic configurations see Table 1). The mechanism by its nature accounts for the increasing reactivity of the excited metal atoms. In the resonance interaction (RI) model,[34−36] the parameters in the Arrhenius rate equation are estimated by taking into consideration the ionization potential and the 4s−4p excitation energy of the metal atom, the electron affinity of the N_2O molecule, and the bond energy of the MO molecule. In particular, in this model the activation barrier depends on the sum of the metal ionization potential and the s−p promotion energy of the metal atom. The model accurately estimates barriers for reactions with alkali and alkaline earth metals[34] but works less successfully for TM atoms,[33] which can be attributed to the neglect of the d electrons in the model.

(37) Herschbach, D. R. *Adv. Chem. Phys.* **1996**, *10*, 319.

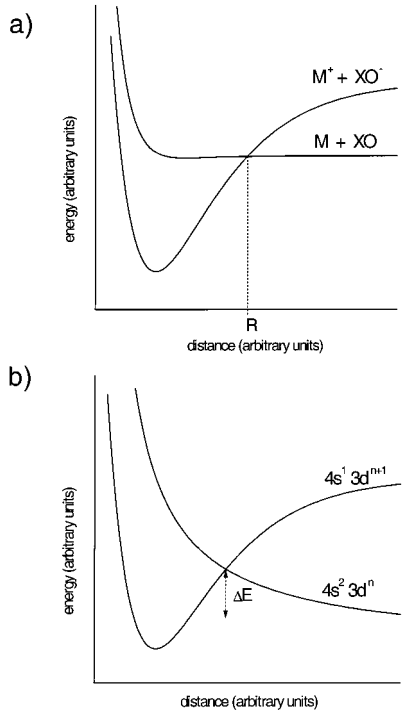

Figure 1. Schematic potential energy curves to illustrate the ET (a) and the DA (b) reaction mechanisms.

Neither of these models provides an overall explanation for the experimentally found trends in the kinetics of reactions 1 and 2 when considering the complete series of the 3d TMs. In two previous studies, I have performed calculations on the reactions of Sc, Ti, and V with N_2O and NO_2.[38,39] In those papers, I attempted to unravel the mechanism of these oxidation reactions for these metals. It was shown that the ET mechanism governs the N−O bond breaking, and during the oxide formation elements of the DA mechanism work. Very recently, the activation barriers for the reactions of TM atoms with N_2O have been estimated by combining B3LYP density functional calculations with the coupled cluster method.[40] A correlation was found between the activation energies and the binding energy of the formed metal oxide.

In this study, the complete set of 3d transition metal atoms (Sc−Ni, open d shell in the neutral state) is considered, and their reactions with N_2O and NO_2 are described and compared.

(38) Stirling, A. *J. Phys. Chem. A* **1998**, *102*, 6565.
(39) Stirling, A. *Chem. Phys. Lett.* **1998**, *298*, 101.
(40) Delabie, A.; Vinckier, C.; Flock, M.; Pierloot, K. *J. Phys. Chem. A* **2001**, *105*, 5479.

Analysis of the calculated potential energy surfaces reveals a novel reaction mechanism which is called the electron-transfer-assisted oxygen abstraction. The main feature of this model is an initial electron transfer followed by 4s−3d hybridization and further electron transfer. In the later stages of the reaction, a net 4s electron transfer takes place via partial excitation and subsequent reorganizations in the metal electron structure. Besides the detailed description of the reaction mechanism, I will provide comparison with the ET and DA kinetic models, which further strengthens the arguments for the proposed reaction mechanism. In addition, the differences between reactions 1 and 2 are also presented and discussed.

II. Computational Details

The potential energy profiles are calculated by solving the Kohn−Sham equations using the B3LYP hybrid functional[41] as implemented in the Gaussian98 program suite.[42] Schäfer's (14,9,5)/[8,5,3] all-electron basis set[43] supplemented with two polarization p functions[44] and a diffuse d function[45] was used for the TM atoms, whereas the 6-311+G-(2d) basis set[42] was chosen for the N and O atoms. The diffuse functions proved to be indispensable to reproduce the electron affinities of the nitrogen−oxides. This is very important in the proper description of the electron transfers occurring in the reactions. The basis set superposition error (BSSE) was estimated in several stages of the reactions. It was found that this error is always smaller than 3 kcal/mol. The algorithm following the reaction coordinate was the steepest descent method. We set the threshold of the maximum atomic displacement to 0.03 au, providing in this way that the optimization can effectively scan the fine details of the potential energy surface. Transition states were characterized by the single negative eigenvalue of the corresponding Hessian. Constrained geometry optimization algorithm was used to follow step-by-step the N−O bond breaking when different reaction paths were available. Atomic energies are calculated using nonspherical electron densities and integral numbers for the atomic orbital occupancies.

Before going into the details of the calculations, it is important to discuss two problems of the density functional theory in calculations of transition metal atoms. It is known that present day functionals are not invariant over the set of densities which belong to the same degenerate ground state; therefore, different occupancies corresponding to the same atomic state can lead to different energies.[46] It has been also known that the current functionals unduly favor the 3d-rich ($4s^1$-$3d^{n+1}$) configurations.[47−50] This problem, which is primarily due to the large correlation energy associated with 3d electrons, renders the accurate estimation of the $4s^23d^n \rightarrow 4s^13d^{n+1}$ excitation very difficult. In the present work, the reaction energies have been obtained with those atomic orbital occupations which lead to the lowest energy. It is important to note that the above difficulties are significantly attenuated when the TM atoms are incorporated into molecules and the symmetry of the complete system is low (usually Cs or often lower in our cases).

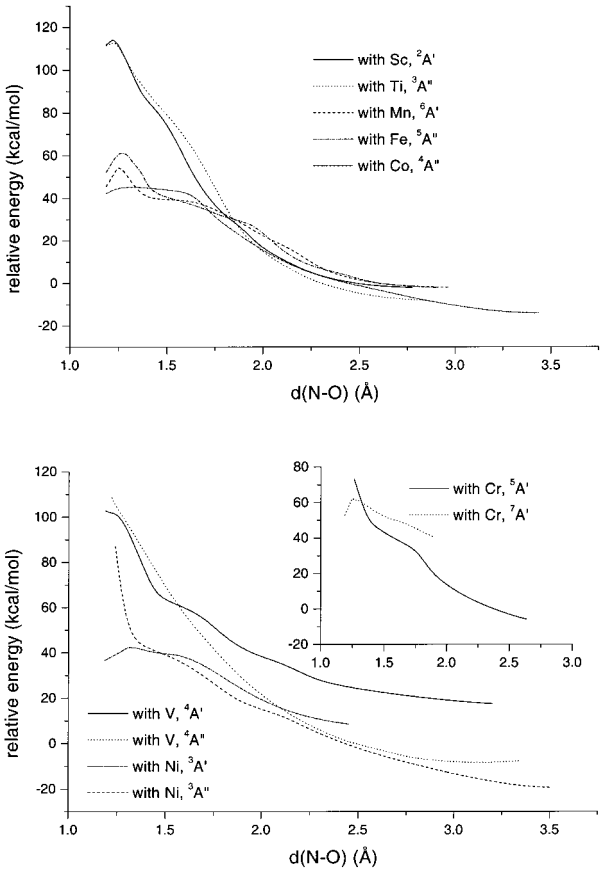

Figure 2. Reaction energy curves for the 3d transition metal atoms and N_2O reactions.

III. Results

A. Microscopic Mechanism. 1. Energetics. The calculated ground-state energy curves for the 3d atoms are plotted in Figures 2 and 3 for N_2O and NO_2, respectively. The metal atom and the reacting NO_x molecule can approach each other in different arrangements. For N_2O, the reaction taking place from a side-on $\eta^2_{N,O}$ approach is depicted. The calculations showed that the collinear geometry is much less favorable, and the oxygen abstraction requires much more optimization to take place if it occurs at all. This observation is in accord with the results of refs 51 and 52, where it was shown for the $O(^1D) + N_2O(^1\Sigma^+)$ and the $Mg(^1S/^3P) + N_2O(^1\Sigma^+)$ reactions that the reaction channels are strongly noncollinear. The preference of noncollinear directions indicates that the inefficiency of the N_2O reactions can be related to the fact that the majority of the collisions are elastic from unsuited entrance angles toward the N−O bond, besides the resultless collisions with the inert N_2 part of the molecule. In the present paper the study is restricted to the examination of the effective channel. For NO_2, the side-on $\eta^2_{N,O}$ (either in-plane or out-of-plane), the end-on η^1_O, and the $\eta^2_{O,O}$ directions are the likely initial configurations in

(41) Becke, A. D. *J. Chem. Phys.* **1993**, *98*, 5648. Lee, C.; Yang, W.; Parr, R. G. *Phys. Rev. B* **1988**, *37*, 785.
(42) Frisch, M. J.; Trucks, G. W.; Schlegel, H. B.; Scuseria, G. E.; Robb, M. A.; Cheeseman, J. R.; Zakrzewski, V. G.; Montgomery, J. A., Jr.; Stratmann, R. E.; Burant, J. C.; Dapprich, S.; Millam, J. M.; Daniels, A. D.; Kudin, K. N.; Strain, M. C.; Farkas, O.; Tomasi, J.; Barone, V.; Cossi, M.; Cammi, R.; Mennucci, B.; Pomelli, C.; Adamo, C.; Clifford, S.; Ochterski, J.; Petersson, G. A.; Ayala, P. Y.; Cui, Q.; Morokuma, K.; Malick, D. K.; Rabuck, A. D.; Raghavachari, K.; Foresman, J. B.; Cioslowski, J.; Ortiz, J. V.; Stefanov, B. B.; Liu, G.; Liashenko, A.; Piskorz, P.; Komaromi, I.; Gomperts, R.; Martin, R. L.; Fox, D. J.; Keith, T.; Al-Laham, M. A.; Peng, C. Y.; Nanayakkara, A.; Gonzalez, C.; Challacombe, M.; Gill, P. M. W.; Johnson, B. G.; Chen, W.; Wong, M. W.; Andres, J. L.; Head-Gordon, M.; Replogle, E. S.; Pople, J. A. *Gaussian 98*; Gaussian, Inc.: Pittsburgh, PA, 1998.
(43) Schäfer, A.; Horn, H.; Ahlrichs, R. J. *J. Chem. Phys.* **1992**, *97*, 2571.
(44) Wachters, A. J. H. *J. Chem. Phys.* **1970**, *52*, 1033.
(45) Hay, P. J. *J. Chem. Phys.* **1977**, *66*, 4377.
(46) Baerends, E. J.; Branchell, V.; Sodupe, M. *Chem. Phys. Lett.* **1997**, *265*, 481.
(47) Gunnarson, O.; Jones, R. O. *Phys. Rev. B* **1985**, *31*, 7588.
(48) Kutzler, F. W.; Painter, G. S. *Phys. Rev. B* **1991**, *43*, 6865.
(49) Russo, T. V.; Martin, R. L.; Hay, P. J. *J. Chem. Phys.* **1994**, *101*, 7729.
(50) Salahub, D. R. *Adv. Chem. Phys.* **1987**, *69*, 447.
(51) Last, I.; Aguilar, A.; Sayós, R.; González, M.; Gilibert, M. *J. Phys. Chem.* **1997**, *101*, 1206.
(52) Yarkony, D. R. *J. Chem. Phys.* **1983**, *78*, 6763.

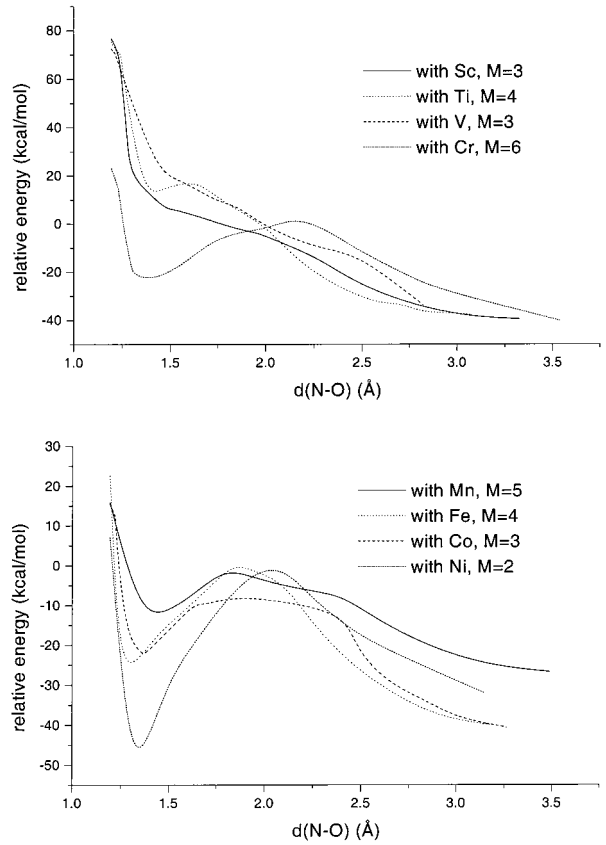

Figure 3. Reaction energy curves for the 3d transition metal atoms and NO_2 reactions starting from an out-of-plane $\eta^2_{N,O}$ configuration. *M* indicates the multiplicity of the surfaces.

reaction 2. The reactions starting from the out-of-plane $\eta^2_{N,O}$ geometry are shown in Figure 3 because this arrangement has the largest probability among the collision directions. Since different internal coordinates dominate the reaction coordinate as the reactions proceeds, it is not obvious how to plot the reaction curves. The breaking N−O bond distance is selected for the horizontal axes in Figures 2 and 3. (In other words, the reaction coordinate is projected onto the N−O internal coordinate as a rational choice for processes involving N−O bond cleaving.) Notice, however, that the shape of the curves often indicates that other internal coordinates also change considerably at certain regions. The energy scale of the figures is given relative to the total energy of the reaction products at infinite separation. As we will see, both types of reactions leading to metal−oxide formation can take place on spin-conserving routes, except when the TM atom is chromium. This is related to the fact that the occupancy of the d shell in ground-state Cr is derived from the $4s^13d^5$ state instead of the $4s^23d^4$, due to the well-known preference of half-full occupations. (See Table 1 for the electron configurations.) The reactions with NO_2 were found to proceed on a single curve for a given spin state. In contrast, reactions of V and Ni with N_2O take place on surfaces belonging to different symmetry representations. Note that the study is restricted to investigate the ground-state curves, and the complete description of every low-lying surface is beyond the scope of the present study. The most important energy values characterizing the transition states and the exothermicity of the reactions are summarized in Tables 2 and 3.

Figure 2 shows that all reactions except reaction with V go through an activation barrier in the initial stage. The ZPVE

Table 2. Characterization of the Transition States for the Reactions of TM Atoms with N_2O (ZPVE Corrections Are Included)

atom	E_a (calcd)	E_a (exptl)[a]	M–O (Å)	O–N–N (°)	ν_1[b]	ν_2[c]
Sc	1.17	2.87	2.340	173	394i	93
Ti	0.42	3.42	2.232	171	350i	97
V	−2.32	2.56	2.272	168	295i	118
Cr	7.90	5.04	2.536	155	233i	93
Mn	7.71	10.68	2.336	150	288i	92
Fe	4.27	10.61	2.067	150	309i	114
Co	2.48	11.66	2.053	148	249i	158
Ni	2.06	2.70	2.011	150	223i	162

[a] Experimental data from ref 33. [b] Imaginary frequencies corresponding to the reaction routes going through the barrier (mix of M−O and N−O stretchings and O−N−N bending). [c] The corresponding normal mode describes the displacement of the metal atom parallel with the N−O axis (M−O−N bending).

Table 3. Reaction Energies and Stabilities of the Final Complexes (kcal/mol) (Experimental Values Compiled from Refs 54 and 57 Are in Parentheses; ZPVE Corrections Are Included)

	atom	reaction energy[a]	stability of the final complex[b]
N_2O	Sc	113.9 (119.5)	2.32
	Ti	113.3 (117.5)	2.29
	V	104.8 (106.4)	0.20
	Cr	55.0 (59.6)	7.35
	Mn	47.7 (46.3)	3.76
	Fe	54.4 (54.1)	−
	Co	44.5 (48.8)	8.22
	Ni	39.0 (48.1)	13.5
NO_2	Sc	83.4 (88.5)	34.3
	Ti	82.9 (86.5)	32.3
	V	74.4 (75.4)	28.2
	Cr	24.5 (28.6)	34.8
	Mn	17.3 (15.3)	21.2
	Fe	24.0 (23.1)	34.3
	Co	14.1 (17.8)	37.8
	Ni	8.5 (17.1)	31.5

[a] Calculated as the difference between the energy of the isolated products and the initial reagents. Experimental values[57,54] are in parentheses. [b] Calculated as the difference between the energy of the optimized final complex and the isolated products. For the reaction between Fe and N_2O, final $OFe-N_2$ formation was not observed.

(zero-point vibrational energy)-corrected barriers, the corresponding experimental values, and selected structural and vibrational parameters for the transition states are collected in Table 2. In the case of Cr, both the quintet and septet curves are presented in the inset. Looking at the inset, it is seen that at the crossing point the N−O bond is somewhat longer than in the activated state, which indicates that the intersection of the two surfaces does not require additional activation. For V and Ni, the symmetry of the transition states and the final states was obtained to be different, which implied that the reactions occur on two surfaces of the same spin state, which cross. Also in these cases, the intersections appear after the transition states and do not involve extra activation energy. The curves demonstrate the large exothermicities of all reactions which are due to the very stable N_2 and the metal−oxide bond formation. The reaction enthalpies are enhanced by the final, weak complex formation between the metal−oxide and the N_2 molecules. The calculated activation energies in most cases show only qualitative agreement with the experimental values. The mean absolute deviation is 3.7 kcal/mol (which is comparable with the BSSE), although for Fe and Co we obtained much lower values than the experiment and for V the calculations did not predict an activation barrier. However, for reactions with TM atoms, this kind of agreement should be considered good because the atomic states of the atoms cannot be described more accurately.

Table 4. Structural Properties of the Insertion Products of Reaction 4: Bond Lengths in Angstroms, Bond Angles in Degrees

atom M	d(M–O) (d_0(M–O))[a]	d(N–O)	d(M–N)	α(OMN)	α(MNO)
Sc	1.689 (1.669)	1.203	2.066	124.4	167.1
Ti	1.629 (1.621)	1.190	1.968	116.7	165.1
V	1.600 (1.589)	1.184	1.820	111.0	166.2
Cr	1.616 (1.622)	1.174	1.921	180.0	180.0
Mn	1.638 (1.642)	1.164	1.849	180.0	180.0
Fe	1.644 (1.619)	1.172	1.758	140.3	160.0
Co	1.627 (1.632)	1.170	1.759	180.0	180.0
Ni	1.611 (1.635)	1.163	1.728	180.0	180.0

[a] The M−O distance in the insertion product is compared with the theoretical M−O bond lengths (in parentheses) in the corresponding oxide molecule. For comparison, the calculated N−O distance in a NO molecule is 1.147 Å.

Furthermore, in real situations the reactants have finite kinetic energy, which may force them to follow other, less favorable routes. This also contributes to the discrepancy between theory and experiment. Notice that the calculated values compare well with those obtained in ref 40, owing to the similarity of the computational methods. The structural and vibrational data presented in Table 2 provide additional information about the transition states. Going from Sc to Ni, the M−O distance shortens in the transition state (except for Cr due to its half-filled valence shell in the septet state), while the bending of the N_2O molecule becomes more and more pronounced. In all cases, the transition state is represented with an imaginary frequency with large absolute value. It is interesting to see, however, that the lowest real frequency describing the displacement of the metal atom along an axis parallel with the N−O bond is very low, indicating a very wide entrance channel for the reactions from the direction perpendicular to the N−O bond.

The curves in Figure 3 show interesting behavior. While for Sc and V smooth, barrierless curves were obtained, for all the other six metal atoms the reaction paths exhibited minima and maxima along the N−O bond-breaking coordinate. For Ti the minimum is an $\eta^2_{N,O}$ Ti−NO_2 complex, whereas in the cases of Cr, Mn, Fe, Co, and Ni the reactions start with a planar $\eta^2_{O,O}$ complex formation. These reactions then proceed by going over a barrier. The height of the barriers does not exceed the energy of the reactants, which means that activation is not necessary for these processes. The reactions with NO_2 have smaller reaction energies than those with N_2O, as seen from Table 3. The metal−oxide and NO reaction products form very stable complexes in each case, much stronger than in the reactions with N_2O. The bond strength between the metal atom and the NO molecule is so large that reaction 2 in fact can be written as an insertion reaction:

$$M + NO_2 \rightarrow ON{-}MO \qquad (4)$$

The metal atom inserts into one of the N−O bonds of the NO_2 molecule. In each case, expect for Ni, the strength of the initial M−NO_2 complex is smaller than the strength of the final oxo−nitrosyl complex. In contrast, the $\eta^2_{O,O}$ complex between a Ni atom and a NO_2 molecule is more stable than the product of eq 4, which predicts that in the case of Ni the real product of the reaction with NO_2 will be the Ni−NO_2 complex instead of the insertion compound. Table 4 presents the structural properties of the final insertion complexes for each atom. In all cases, the symmetry of the products was C_s or higher ($C_{\infty v}$). According to the calculations, the oxo−nitrosyl complexes can be bent or linear. There is an apparent correlation between the M−O bond length changes with respect to the original MO bond distances and the fact that the complex is linear or bent. If the complex is bent (Sc, Ti, V, and Fe), the M−O distances are increased by the nitrosyl complex formation, while in the linear complexes the M−O lengths are shorter than in the corresponding MO molecules. In each case the NO ligand is activated, as shown by the lengthened (and weakened) N−O bond. The metal−nitrogen distances decrease downward following the size of the atoms.

Table 3 shows that the calculated reaction energies compare well with the experimental entries. The mean absolute deviation is 3.9 kcal/mol for the reactions with N_2O and 3.6 kcal/mol for the NO_2 cases. This agreement with experiment is very good for transition metal systems. Note that these deviations are comparable with that obtained for the activation barriers.

2. Orbital Aspects. What are the most important electronic factors which govern reactions 1 and 2? Inspection of the orbital structures in several stages of the reactions reveals similar mechanisms for the two nitrogen−oxides. In the following, the original orbital symmetry names (s, d, σ, π) will be used, although during the reactions this notation is not valid because the whole symmetry of the reacting systems is radically reduced.

N_2O. All the reactions are initiated by electron transfer from the metal atoms to the N_2O empty 3π (LUMO) orbital. (The charge transfer can be observed either by inspecting the shape and composition of the new molecular orbitals or by estimating partial charges (e.g., Mulliken or other partial charge schemes), as was carried out in refs 38 and 39.) This charge transfer has three essential consequences: (a) population of the N_2O LUMO destabilizes both the N−N and, more importantly, the N−O bonds because this orbital has antibonding character for these bonds; (b) the N_2O molecule starts to bend because the optimal structure of a negatively charged N_2O is bent-shaped; and (c) the metal−oxide 3π orbital starts to form from this charge transfer. Inspection of the orbital overlaps in the transition states shows that the extent of the electron donation is increasing when going from Sc to Ni. This is consistent with the decrease in the NNO bond angles in Table 2. (See also ref 40, where this trend has also been observed.) From the size and shape of the metal atomic orbitals, it is expected that the 4s orbitals dominate the initial charge transfer. It is surprising, however, that often the 3d orbitals also play a role in the charge transfers by forming hybrid orbitals with the 4s orbital (Sc, V, Cr, Mn, and Fe). As the reactions further proceed, charge transfer starts to take place in the opposite direction; namely, the HOMO of N_2O (2π) populates an empty 3d metal orbital available by symmetry. This orbital overlap is responsible for the formation of the 8σ metal−oxide orbital and for the additional weakening of the N−O bond, because the HOMO is bonding for the N−O bond. For all metals expect Ni, the $4s^\beta$ atomic orbital rapidly becomes empty via charge transfer from 4s−3d hybrid metal orbitals toward the N_2O in a relatively early stage of the reactions. Although in both CoO and NiO the metal atoms keep both s electrons in their atomic asymptotes (see Table 1), the calculations showed that, for Co, the $4s^\beta$ electron is transferred to a 3d orbital in the final complex, resulting in a slightly excited CoO asymptotic state. After the transition state, further overlaps between metal 3d and N_2O orbitals become more and more

pronounced. Due to the mutual electron transfers, the N−O bond is further destabilized and then breaks, and the formation of the metal−oxide bond takes place simultaneously. In the final stage of the reactions, the weak N_2−MO complex is formed, and the oxide and N_2 formations are completed. The N_2 and MO parts of the final complex are only weakly perturbed by the complex formation, as indicated by their slightly lengthened bonds. In the case of V and Ni, crossing of the A′ and A″ surfaces (within the same spin state) is necessary to facilitate the ground-state oxide formation.

NO_2. Similarly to the N_2O cases, the reactions start with an electron transfer toward the empty 3π NO_2 orbital. This orbital has antibonding nature on both N−O bonds; therefore, this charge flow weakens the N−O interactions. A charge back-donation starts from the SOMO of NO_2 toward an empty 3d metal orbital also in the early stage of the reactions. This also weakens the attacked N−O bond, because the SOMO has bonding character for this bond. As the metal atom approaches the N−O axis, further orbital overlappings take place, and the attacked N−O bond breaks. In this region of the potential energy surface, the original $4s^{\beta}$ metal orbital rapidly becomes empty via a 3d−4s hybrid orbital in the cases of Sc, Ti, V, Cr, Mn, Fe, and Co, similarly to the N_2O cases. This gives rise to an excited CoO asymptote for Co. By contrast, for Ni significant overlap forms only between the 4s−3d hybrids and the N−O LUMO orbitals for both spin manifolds. Simultaneously, the metal−oxide bond gradually becomes strong, and then the bond formation is completed due to further overlaps between the NO_2 and 3d metal orbitals. The NO and the MO parts form the final, quite strong complex via $2\pi^*-4\pi^*/1\delta$ orbital interactions. To facilitate this interaction, Sc also takes up an excited asymptotic state by promoting its $4s^{\alpha}$ electron to a 3d state, as was already shown in ref 39.

Let us now consider the final nitrosyl complexes from the electronic point of view. At first glance, it is not obvious why the complexes with more d electrons are linear, whereas in the cases of Sc, Ti, and V (as well as Fe, but it is an exception) we obtained bent structures. Naively, one expects larger repulsion between the NO orbitals and the MO part when more d electrons are on the metal atom, and bending would effectively reduce such repulsion. This is the mechanism for simple M−NO nitrosyls in their ground states:[53] the nitrosyl complexes are linear for Sc, Ti, V, Cr, and Fe, whereas they take a bent shape for Mn, Co, and Ni. Inspection of the orbitals reveals that the most important interaction which is responsible for the linearity of the products is the overlap between the $2\pi^*$ orbitals of NO and the $4\pi^*$ orbitals of the metal−oxide part (the asterisk indicates the antibonding nature of the orbitals). NO has one electron on one of its $2\pi^*$ orbitals. Without discussing the electronic structure of the oxides in detail (see, e.g., ref 54; note that the calculations nicely reproduced the ground-state configurations for the oxides), we recall that for Sc, Ti, and V the antibonding $4\pi^*$ orbital is empty, while in the other oxides this orbital is occupied by either one or two electrons. The overlap between the metal−oxide $4\pi^*$ and the NO $2\pi^*$ is maximized in linear arrangement, while in a bent state this interaction is not so efficient. Electron donation from NO to the $4\pi^*$ orbital is unfavorable when it is completely empty because this weakens the metal−oxide interaction. Therefore, the complexes of Sc, Ti, and V take bent conformation in order to avoid the large overlap. Still, this reduced overlap results in slight elongation in the M−O bonds, as compared to the corresponding metal−oxide bond length. By contrast, when the $4\pi^*$ orbitals are occupied, the maximized overlap with the NO $2\pi^*$ orbitals facilitates charge transfer toward the empty NO $2\pi^*$ orbitals, because in this way the occupancy of the antibonding $4\pi^*$ orbitals can be decreased and the M−O bond strengthens. The shortened M−O distances nicely illustrate this mechanism. Again there is an exception, Fe. In this case, our calculations showed that the OFe−NO complex has one imaginary frequency in its linear state, forcing the molecule to bend. This motion is coupled with a reorganization in the electronic structure, namely a $1\delta-4\pi^*$ transition in the metal−oxide part, for which the bent conformation is more favorable.

The common electronic and structural features prompt us to formulate a general reaction mechanism: the reactions are initiated by electron transfer playing a multiple role and then proceed via overlaps between 3d/3d−4s metal hybrid and nitrogen−oxide orbitals. Simultaneous N−O bond breaking and M−O formation occur during the reactions, accompanied by a final complex formation between the products. In brief, both the ET and the DA mechanisms play roles in the reaction courses. Note that the pattern of the common transition metal−ligand interaction (π-donation, back-donation) bears a resemblance to this mechanism.

B. Discussion. If we artificially divide reactions 1 and 2 into an N−O bond-breaking step and a metal−oxide formation step, we have the following spin-conserving routes:

$$N_2O(^1\Sigma^+) \rightarrow N_2(^1\Sigma_g^+) + O(^1D) \quad (5)$$

$$NO_2(^2A_1) \rightarrow NO(^2\Pi) + O(^3P) \quad (6)$$

$$^{7-|n-4|}M + O(^3P) \rightarrow {}^{6-|n-5|}MO \quad (7)$$

$$^{7-|n-4|}M + O(^1D) \rightarrow {}^{6-|n-5|}MO \quad (8)$$

Equation 7 is valid for Sc−Cr, whereas eq 8 is valid for Mn−Ni in both types of reactions. The $7-|n-4|$ and $6-|n-5|$ formulas are simple and concise expressions for the multiplicities of the metal atomic asymptotes in the oxides and the multiplicities of the metal−oxides, respectively, as derived from Table 1. Here $n = 1, 2, ..., 8$ going from Sc to Ni. We have two basic problems that are often pointed out in connection with reactions 1 and 2, and these problems are essentially related to the question of spin conservation:[5−7,10,12,13,17,21]

(i) Reactions 5 and 6 underline a significant difference between N_2O and NO_2. While NO_2 decomposition produces ground-state, reactive $O(^3P)$ atoms on the adiabatic surface, the spin-conserving, diabatic dissociation of N_2O yields an unreactive, excited-state $O(^1D)$, well above the adiabatic $N_2(^1\Sigma_g^+) + O(^3P)$ surface. From eq 7 we can see that Sc, Ti, V, and Cr require $O(^3P)$ atom for oxide formation. The $O(^1D)$ state correlates with high-energy excited MO states in their cases. In contrast, the Mn−Ni group has the ^1D oxygen asymptote in their oxide forms. So it is clear that the spin-conserving dissociation of N_2O and NO_2 provides an oxygen atom in an atomic state suitable only for a smaller group of 3d TM atoms in each case, not for all metals.

(53) Balnchet, C.; Duarte, H. A.; Salahub, D. R. *J. Chem. Phys.* **1997**, *106*, 8778.
(54) Merer, A. J. *Annu. Rev. Phys. Chem.* **1989**, *40*, 407.

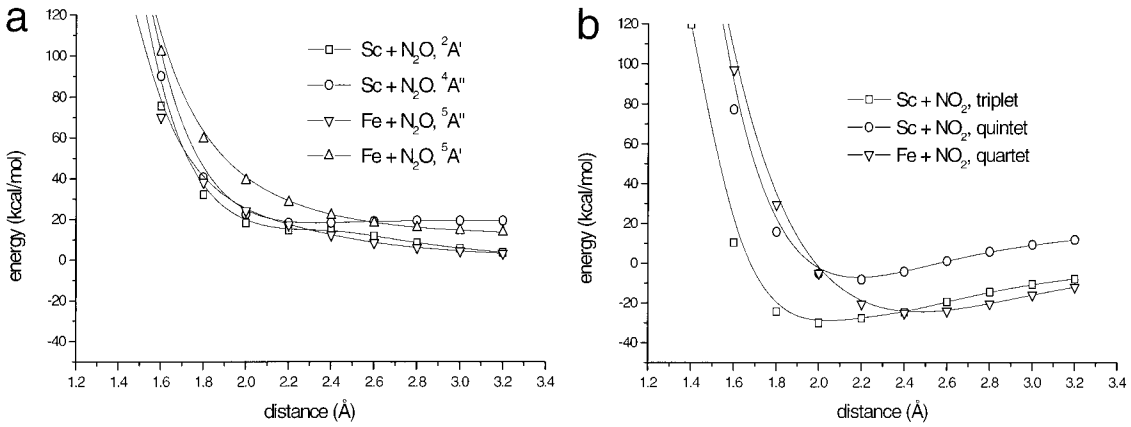

Figure 4. Interaction curves for ground- and excited-state Sc and Fe atoms with unperturbed N_2O (a) and NO_2 (b) molecule. Note that (a) curves with NO_2 generated for out-of-plane approach of the metal atoms; (b) in the case of Fe + NO_2 only the ground-state curve is given because the excitation is not accompanied by spin change. Energy scales are relative to the total energy of the ground-state atom plus the energy of the nitrogen−oxide. Lines are guides to the eyes.

(ii) It is seen that the atomic asymptotes are derived from the first excited-state configurations, except for Cr and Co. Note that the transition between the $4s^23d^n$ and $4s^13d^{n+1}$ configurations does not require a change in multiplicity for Mn−Ni, but it does for the metals in the first half of the 3d row (the $7 - |n - 4|$ and $6 - |n - 5|$ expressions in both eqs 7 and 8 take the same values for $n = 5-8$). It follows that for Sc, Ti, and V, oxide formation by reaction 7 is accompanied by a change in the atomic multiplicities, and this is true for chromium owing to the septet−quintet transition.

Comparison of eqs 5−8 and Table 1 therefore clearly shows that the spin-conserving N−O bond-breaking and metal−oxide formation steps cannot be coupled in a simple, straightforward way. On the other hand, the complete reactions are not spin-forbidden (not including now the reaction between Cr and N_2O):

$$N_2O(^1\Sigma^+) + {}^{6-|n-5|}M \rightarrow N_2(^1\Sigma_g^+) + {}^{6-|n-5|}MO \qquad (9)$$

$$NO_2(^2A_1) + {}^{6-|n-5|}M \rightarrow NO(^2\Pi) + {}^{6-|n-5|}MO \qquad (10)$$

which strongly suggests that these reactions can proceed without crossing surfaces with different spin multiplicities. (The $6 - |n - 5|$ expression is the general formula to express the multiplicities of the reacting ground-state 3d atoms (first excited state for Cr) and oxides.) The calculations revealed that both reactions 1 and 2 are initiated by an electron transfer from the TM atom to the nitrogen−oxide molecule. It turns out that this is a crucial step in coupling the N−O bond breaking and the metal−oxide bond formation. Due to this charge transfer, the bond-breaking and formation processes occur on the following spin-conserving routes:[55]

$$N_2O^-(^2A') \rightarrow N_2(^1\Sigma_g^+) + O^-(^2P) \qquad (11)$$

$$NO_2^-(^1A_1) \rightarrow NO(^2\Pi) + O^-(^2P) \qquad (12)$$

$${}^{7-|n-5|}M^+ + O^-(^2P) \rightarrow {}^{6-|n-5|}MO \qquad (13)$$

In eq 13, the $7 - |n - 5|$ expression stands for the multiplicities of the ionic asymptotes of the metal atoms (Table 1), which are derived by employing the fact that the metal−oxide bonds are ionic. It is clear from Table 1 that all oxides have a ^2P oxygen anionic asymptote, and this is the state of the oxygen anion yielded by the N_2O^- or NO_2^- decomposition. Equations 11−13 thus demonstrate that the dissociation of the charged nitrogen−oxide molecules can be connected to the metal−oxide formations without any intersystem crossing. This underlines the importance of the charge transfer during the reactions: in this way the dissociation of the nitrogen−oxides is directly coupled to the M^+O^- formation without barrier coming from surface crossings due to altering spin states. Although the ionic ground states for Co an Ni differ from the states given by the above formula, their actual ionic ground states can also be connected to the oxide formation without surface crossing.

To emphasize the importance of the electron transfer in reactions 1 and 2, Figure 4 is presented. In this figure the potential energy curves describing the interaction of different ground- and excited-state metal atoms with a N_2O (Figure 4a) or a NO_2 (Figure 4b) molecule are plotted. The geometry of both nitrogen−oxide molecules was fixed at their equilibrium geometry, and the distance between the metal atom and the center of the breaking N−O bond was varied. The curves for Sc and Fe are presented only, for simplicity, but the results are characteristic for the other metals, too. Even at a glance, we can see that the interaction of the metal atoms with a linear N_2O is basically repulsive (Figure 4a), whereas significant interaction energy is obtained with NO_2 (Figure 4b), irrespective of whether the metal atom is in its ground or excited state. This marked difference can be explained by the fact that the vertical electron affinity of N_2O is highly negative, while that of NO_2 is a considerably large, positive value.[55−57] Although the formation of N_2O^- ion is a favorable process (its adiabatic electronaffinity value is positive value), it requires a substantial bending of the N−N−O structure. Since the curves in Figure

(55) Hopper, D. G.; Wahl, A. C.; Wu, R. L. C.; Tiernan, T. O. *J. Chem. Phys.* **1976**, *65*, 5474.

(56) Experimental electron affinites in kilocalories per mole: adiabatic 5.07 (N_2O)[55] and 52.38 (NO_2);[57] vertical estimation −51.42[55] (N_2O). Theoretical estimation: for N_2O, adiabatic 3.53, vertical −35.92; for NO_2, adiabatic 52.43, vertical 27.00; in good agreement with recent calculation (Tschumper, G. S.; Schaefer, H. F., III. *J. Chem. Phys.* **1997**, *107*, 2529.). We note that, according to the convention, a positive electron affinity value indicates favorable negative ion formation, while a negative value indicates that the ion is not stable.[57]

(57) *CRC Handbook of Chemistry and Physics*, 69th ed.; CRC Press: Boca Raton, FL, 1988.

4a are generated by fixing the linearity of the N_2O molecule, the electron transfer is suppressed in these cases. The remaining interaction is repulsive. Hence, we can deduce that neither the ground- nor the excited-state metal atoms are able to interact with N_2O without charge transfer. In other words, electron transfer is indispensable for the reactions. Moreover, the excited-state curves prove that promotion alone is not sufficient for obtaining attractive interaction between N_2O and 3d metal atoms. For NO_2 the situation is remarkably different. Having positive vertical electronaffinity for NO_2, we can infer that the interaction between the metal atoms with NO_2 necessarily involves charge transfer. This underlines the importance of the electron transfer in this case, too. Since the adiabatic electron affinity of NO_2 is much larger than the vertical value, the charge transfer between the metal atom and the NO_2 molecule with fixed geometry is inevitably reduced only.

C. Theory and Experiment. In this section, a detailed comparison between experiment and theory is given which will be of additional value in elucidating the mechanism. Usually it is not straightforward to establish the link between macroscopic data and a microscopic mechanism. The curves in Figures 2 and 3 represent the potential energy variation only in a single, successful encounter from a given reactant arrangement (though several others have been tested). Measured rate constants and activation energies, however, reflect the average of many efficient and inefficient collisions. Efficiency largely depends on numerous parameters such as orientation, relative velocities, etc. Nevertheless, it is reasonable to discuss our findings in terms of the simple kinetic models described in the Introduction. Evaluation of these models in the light of the theoretical results is of primary importance, since these are the kinetic models which are most frequently invoked to account for the experimental observation. In the ET and DA models, the rate constants can be estimated by eqs 14 and 15, respectively:[58]

$$k_{ET} = R_{ET}^2 \pi \sqrt{\frac{8RT}{\pi\mu}} \tag{14}$$

$$k_{DA} = R_{DA}^2 \pi \sqrt{\frac{8RT}{\pi\mu}} e^{-E_a/RT} \tag{15}$$

Here, R_{ET} and R_{DA} are the radii of the cross sections, the square-rooted term is the average molecular velocity, and finally the exponential term in eq 15 is the Boltzmann factor in the threshold (activation) energy. R_{ET} is calculated using eq 3, while R_{DA} is estimated from the rigid-sphere molecular diameters of the reactants. For the DA model, the E_a values are usually set to be the lowest excitation energy of the metal atoms.[6] For 300 K, the k_{ET} and k_{DA} values of the reactions with N_2O are plotted in Figure 5, using experimental data. For comparison, the measured rate constants are also displayed in this figure. It is seen that the ET model predicts quite uniform rate constants. In contrast, the rates calculated using the DA formula show very large variation in order of magnitude, and often unphysically low values are obtained. It is obvious that the Boltzmann factor lowers the DA rates substantially, because the velocity terms are the same and the cross sections are of the same order in eqs 14 and 15. The most important observation which can be made when inspecting Figure 5 is that the experimental rate constant values consistently fall between the ET and DA values. This trend convincingly indicates that the reaction mechanism is composed of ingredients of both the ET and the DA models. In general, the fundamental reason that neither model is able to account for the mechanism alone is, of course, their oversimplified nature. Notwithstanding, further reasoning is given below to rationalize why the pure ET and DA mechanisms over- and underestimate, respectively, the experimental rates.

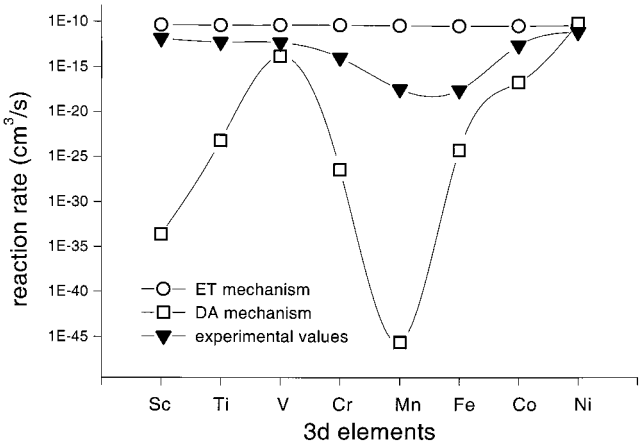

Figure 5. Logarithmic plots of the bimolecular rate constants (measured, and estimated from the ET and DA models) for the reactions of the 3d transition metal atoms with N_2O. For the calculations of the k_{DA}-s, the hard-sphere diameters of the reactants are taken from refs 68−70. Lines are guides to the eyes.

(i) In the ET model we need the metal ionization energy and the electron affinity of the reactant partner, as shown by eq 3. However, the ET approximation breaks down at short internuclear distances.[59−61] This is the case for the reactions with N_2O. When the cross section is small, it is not justified to use either the vertical or the adiabatic electronaffinity values. Furthermore, the electron transfer can occur from different orbitals, and other orbitals are excluded from participating in the charge transfer because of the local symmetry. It follows that the choice of the appropriate ionization energy is not easy and requires knowledge of the mechanism. Vertical electron affinity and higher ionization energy decrease the cross section; adiabatic electron affinity and lower ionization energies yield a longer distance for the electron jump. The situation seems to be different for NO_2, though in this case rate constants are available only for Ti[12] and Fe[29]. The observed rates of oxidation are 0.9×10^{-10} and 1.71×10^{-10} cm^3/s for Ti[12] and Fe[29], respectively. The ET model predicts 1.62×10^{-10} and 1.03×10^{-10} *cm^3/s* values for these metals, which compare nicely with experiment, especially if we take into further account the large uncertainties of the measured values.[12,29] Due to its favorable vertical electron affinity, NO_2 has about twice as large an electron jump distance with 3d metals than N_2O, which emphasizes the increased importance of electron transfer in this case. Additional support for the preference of the ET mechanism comes from reactions of Ca and Sr with NO_2,[31] where the measured rate constants were even slightly larger than those predicted by the ET model.

(58) The equations are derived by applying simple gas−kinetic collision theory.

(59) Bourguignon, B.; Gargoura, M.-A.; Rostas, J.; Taieb, G. *J. Phys. Chem.* **1987**, *91*, 2080.
(60) Goldfield, E. M.; Gislason, E. A.; Sabelli, N. H. *J. Chem. Phys.* **1985**, *82*, 3179.
(61) Goldfield, E. M.; Kosmas, A. M.; Gislason, E. A. *J. Chem. Phys.* **1985**, *82*, 3191.

(ii) In the DA model, the Boltzmann term is very sensitive to the magnitude of the activation energy. Even a small change in the activation energy (a few kilocalories per mole) might result several orders of rate decrease via the exponential dependence. The choice of the E_a value is therefore critical in this model. From the reaction mechanism, it is known that only partial excitations take place during the reactions to facilitate the formation of hybrid orbitals. In most cases this hybridization has a specific role. As is seen from Table 1, metal−oxide formation is accompanied by a $4s^{\beta}$ electron loss from the metal atoms (except Co and Ni, vide infra). However, the initial charge transfer takes place from 4s or 3d−4s hybrid orbitals, and subsequent hybridizations facilitate the required $4s^{\beta}$ transfer. On the other hand, in the reactions of Co and Ni, hybridization also takes place owing to the local symmetry of the reacting environment. In these cases, however, the partial promotion plays no specific role in coupling the atomic state with the metal−oxide electronic state. Nevertheless, in most cases the promotions required for the hybridizations do not follow the lowest excitation energy routes. Therefore, employing the lowest promotion energy value in eq 15 is not appropriate. In addition, the atomic excitation energies are no longer valid when the atom is placed in a reactive chemical environment. This is illustrated qualitatively in Figure 1B, where the ΔE value is necessarily smaller than the original excitation energy. Although smaller E_a values would increase the predicted k_{DA} values, it is very difficult to estimate the degree of the excitation which one should take into account to obtain reliable predictions. A first approximation is that the energy barriers arising due to hopping from one surface to another are roughly proportional to the excitation energy. However, it is more likely that the chemical environment influences the atoms to a quite different extent.

On the basis of the reaction mechanism, it is desirable to establish a correlation between the rates or activation energies and simple measurable quantities. This can be done for the reactions with N_2O only, because of the limited number of experimental data for the oxidations with NO_2. If the ET is the dominant mechanism, the order of the reaction rates for a given OX molecule can be predicted by comparing the metal ionization energies; also for a given metal the electron affinities of the OX molecules determine the rate order. If the DA mechanism governs the rate-limiting elementary step, then the order of the reaction rates can be estimated by considering the excitation energies. It turns out that taking the lowest ionization processes from a 3d orbital provides a good correlation. There are two observations which support this choice: (i) The 3d orbitals play a role in the transition states via 4s−3d hybrids. (ii) It was found that the entrance channel is wide along the M−N−O angle (see the discussion of Table 2, above). It can be shown that displacement of the metal atom along this coordinate toward the N−O bond center increases the 3d contribution in the overlap between the metal and N_2O LUMO orbitals. Below, a comparison is given for the experimental rate constants (300 K), the activation energies of N_2O reactions,[62] and the ionization energies necessary for the removal of a 3d electron from the TM atoms.[63] (Note that Cr is omitted here because its reaction requires additional intersystem crossing.)

$$k_{Co} < k_{Mn} \approx k_{Fe} < k_{Ni} < k_{Ti} \approx k_{V} < k_{Sc} \quad (16)$$

$$E_{Co} > E_{Mn} > E_{Fe} > E_{Ti} > E_{Sc} > E_{V} > E_{Ni} \quad (17)$$

$$I_{Mn} > I_{Co} > I_{Fe} > I_{Ti} > I_{Ni} > I_{V} > I_{Sc} \quad (18)$$

Note that the choice of the 3d ionization energy is arbitrary in some cases due to the large number of electron terms emanating from a given orbital configuration. Here I have deliberately selected the one for V which fits into the experimental order. A very nice picture emerges from this comparison: the rate constant and activation energy orders follow nicely the decreasing order of 3d ionization energies, except that in some cases two atoms have reversed their order. This provides strong additional support for the mechanism. The comparison also demonstrates that precise knowledge of the electronic mechanism enables us to identify the appropriate physical observable in rationalizing the reaction mechanism.

The mechanism discussed here helps to elucidate an aspect of the RI mechanism (see Introduction) advanced by Futerko and Fontijn.[34−36] In this model the reaction barrier is proportional with the sum of the metal first ionization and the lowest s−p excitation energies. For transition metal atoms, the s−p excitations usually have no role in their reactions. Nevertheless, the RI model is often able to predict activation energies for even TM atoms in good agreement with experiment. This can be explained by the fact that ionization from a d shell is equal with ionization from an s shell (this is usually the lowest ionization process) plus an extra excitation to reach the higher ionized configuration. This extra excitation energy is usually smaller than the s−p promotion energy. Nonetheless, the fact that a 3d ionization is also a sum of an ionization and an excitation energy perhaps gives a clue why the validity of the RI model can be extended from alkaline and alkaline earth metals (where s−p promotion is the only possibility) to transition metals.

In light of the results, it is useful to consider further possible experiments which might provide additional information about the reactions. In this context, reactions of 3d TM atoms with CO_2 serve as analogies for both N_2O and NO_2. For CO_2, both gas−kinetic[11,12,21−23,26,27,30,64] and matrix-isolation (MI) studies[65−67] have been conducted. Briefly, it has been found from MI measurements that metals on the left side of the 3d row are able to cleave the C−O bond and insert into it, forming OC−MO type complex molecules, whereas metals at the right side of the row produce $M-CO_2$ complexes without insertion. Given that the activation energies for the gas-phase reactions of TM

(62) Experimental rates and activation energies were compiled from the following papers: Sc, V, ref 21; Ti, ref 12; Mn (extrapolated data for room-temperature rate), ref 16; Fe (extrapolated data for room-temperature rate), ref 16, see also ref 17; Co, Ni, ref 33.

(63) Moore C. E. *Atomic Energy Levels As Derived From the Analyses of Optical Spectra*; U.S. National Bureau of Standards Circ. 467; Government Printing Office: Washington, DC, 1949; Vol. 1. Ionization energies in electron-volts: Sc, 8.0; Ti, 9.9; V, 8.7; Mn, 14.3; Fe, 10.8; Co, 13.0; Ni, 8.8.
(64) Campbell, M. L. *Phys. Chem. Chem. Phys.* **1999**, *1*, 3731.
(65) Galan, F.; Fouassier, M.; Tranquille, M.; Mascetti, J.; Pápai, I. *J. Phys. Chem.* **1997**, *101*, 2626.
(66) Pápai, I.; Mascetti, J.; Fournier, R. *J. Phys. Chem.* **1997**, *101*, 4465.
(67) Mascetti, J.; Galan, F.; Pápai, I. *Coord. Chem. Rev.* **1999**, *190−192*, 557.
(68) Hirschfelder, J. O.; Curtis, C. F.; Bird, R. B. *Molecular Theory of Gases and Liquids*; Wiley: New York, 1954.
(69) Barua, A. K.; Rai Dastidar, T. K. *J. Chem. Phys.* **1965**, *43*, 4140.
(70) Fischer, C. F. *The Hartree−Fock Method for Atoms*; Wiley: New York, 1977.
(71) Langhoff, S. R.; Bauschlicher, C. W., Jr. *Annu. Rev. Phys. Chem.* **1988**, *39*, 181.

atoms with CO_2 and N_2O are similar or they are larger for CO_2,[11,12,21,26] but the exothermicity of the N_2O reactions is much larger, it is expected that reaction 1 with ground-state TM atoms can be also observed under MI circumstances. For NO_2, we can also expect reactions and formation of exoergic insertion products as eq 4 dictates. Although energetically accessible, insertion reactions for Ni with NO_2 presumably will not take place because the predicted barriers span a very large reaction coordinate region involving significant structural changes and because the $\eta^2_{O,O}$ intermediate product is more stable than the final insertion compound. Thus, stable Ni−NO_2 complex formation is expected to be observed.

In conclusion, the general reaction mechanism which works during the oxidation reactions of the 3d metal atoms with N_2O and NO_2 is governed by both electron transfer and partial excitation on the metal atom. I call these reactions electron-transfer-assisted oxygen abstraction, emphasizing the importance of both simple kinetic models in the mechanism.

IV. Summary

Reactions of ground-state 3d TM atoms with N_2O and NO_2 are modeled by means of density functional theory. The calculations revealed that the reactions are initiated by an electron transfer from the metal atom to the oxidant molecule, assisting the N−O bond weakening and the $O^-(^2P)$ abstraction to the metal atom without surface crossing. Charge back-donation from the oxidant to the metal atom follows, forming additional bonds between the reactants. Significant 4s−3d hybridization takes place on the metal atom, facilitating in this way a net $4s^\beta$ electron transfer to the nitrogen−oxide molecule. It was shown that the N−O bond breaking and the M−O bond formation is coupled without crossing of surfaces belonging to different spin states (except for Cr). The reaction mechanism postulated for both the N_2O and NO_2 reactions involves the principal motifs of the ET and the DA kinetic models. A suitable name, electron-transfer-assisted oxygen abstraction, is proposed for the mechanism. The pattern of the mechanism indicates that the key steps (mutual charge transfers with multiple role, s−d hybridization to facilitate the appropriate orbital configuration, etc.) operating during the reaction course may govern other oxidation reactions of TM atoms, where the oxidant molecules can be CO_2, SO_2, O_2, NO, or CO.

It was also shown that the structure of the final insertion products in reaction 4 can be rationalized by considering the occupancy of the $4\pi^*$ antibonding metal−oxide orbitals.

Acknowledgment. The author thanks M. L. Campbell for sending his manuscript and Imre Pápai for critical comments. Technical help from G. Schubert is acknowledged. Financial support from the Hungarian Research Foundation (OTKA, Grant No. F025490) and the Bolyai Fellowship is gratefully acknowledged.

JA0118946